

The QCD Equation of State with $N_f = 3$ flavours up to the electro-weak scale

Matteo Bresciani^{a,b}, Mattia Dalla Brida^{a,b}, Leonardo Giusti^{a,b}, and Michele Pepe^b

^a *Dipartimento di Fisica, Università di Milano-Bicocca, Piazza della Scienza 3, I-20126 Milano, Italy*

^b *INFN, Sezione di Milano-Bicocca, Piazza della Scienza 3, I-20126 Milano, Italy*

(Dated: January 22, 2025)

The Equation of State of Quantum Chromodynamics with $N_f = 3$ flavours is determined non-perturbatively in the range of temperatures between 3 and 165 GeV with a precision of about 0.5-1.0%. The calculation is carried out by numerical simulations of lattice gauge theory discretized à la Wilson with shifted boundary conditions in the compact direction. At each given temperature the entropy density is computed at several lattice spacings in order to extrapolate the results to the continuum limit. Taken at face value, data point straight to the Stefan-Boltzmann value by following a linear behaviour in the strong coupling constant squared. They are also compatible with the known perturbative formula supplemented by higher order terms in the coupling constant, a parameterization which describes well our data together with those present in the literature down to 500 MeV.

Introduction — The Equation of State (EoS) of Quantum Chromodynamics (QCD) describes the collective behaviour of strongly-interacting particles at equilibrium. It is of absolute interest in particle and nuclear physics, and in cosmology where it plays a crucial rôle in many physical processes. It has contributed to the evolution of the effective numbers of degrees of freedom in the thermal expansion of the Universe, see Refs. [1, 2] for a recent discussion and reference therein. The evolution during the QCD epoch may have left distinctive features in the spectrum of the primordial gravitational waves background [2], or may have affected significantly the abundance of dark matter candidates, e.g. WIMPs [3–5] and/or axions [6, 7]. In terrestrial laboratories, QCD matter under extreme conditions is produced and investigated at heavy-ion colliders, where the EoS is an essential input in the analysis of data.

At present, the EoS of QCD at zero chemical potential is known up to temperatures of about 1 GeV and with a precision of a few percent. It has been computed non-perturbatively by extrapolating to the continuum limit lattice QCD results with $N_f = 2 + 1$ [8–10] and $N_f = 2 + 1 + 1$ [6] flavors. Above 1 GeV, the EoS is known only perturbatively as a function of the strong coupling constant g . Its expansion has been computed up to order $g^6 \log(g)$, after which the non-perturbative terms from the ultra-soft modes start to contribute [11, 12], see Ref. [13] for recent progress in this field. The convergence of the expansion, however, turns out to be very poor, and the perturbative expression remains insufficient to achieve reliable and precise cosmological predictions [2]. On the theoretical side, the calculation of the EoS in the SU(3) Yang–Mills theory showed that the contributions computed in perturbation theory are very far from explaining the full result even at temperatures as high as the electro-weak scale [14, 15]. More recently, the non-perturbative computation of the QCD screening masses showed that the known perturbative results do not provide a satisfactory description up to these high temper-

atures [16, 17]. All these results indicate that, for a reliable and precise determination of its thermal properties, a fully non-perturbative treatment of QCD is required up to temperatures much higher than 1 GeV.

The purpose of this Letter is to compute the EoS of QCD non-perturbatively over a wide range of temperatures T from 3 GeV up to the electro-weak scale. The computational strategy is entirely new, and we focus on the theory with $N_f = 3$ flavours of massless quarks. This choice is justified since the effect of the masses of the 3 lightest quarks is negligible within errors in the explored range of temperatures [6, 10, 18]. At the same time, the strategy adopted is fully general and can be applied to QCD with five (massive) quarks without further conceptual difficulties.

This progress is achieved by extending and applying to the EoS a recently proposed strategy for studying QCD up to very high temperatures from first principles [16]. The key novelties with respect to the standard “integral” method are: (a) abandon the hadronic scheme to renormalize the theory, and determine the lines of constant physics by fixing the value of a non-perturbatively defined renormalized running coupling computed at very different scales by using step-scaling techniques [19–21], (b) avoid the zero-temperature subtraction of the ultraviolet power divergence in thermodynamic potentials by computing directly the entropy density s in a moving reference frame formalized by shifted boundary conditions [22–25]. The pressure p can then be computed by integrating the entropy in the temperature, while the energy density e is determined by integrating the temperature in the entropy or, equivalently, by using the relation $Ts = (e + p)$.

Preliminaries — We regularize QCD on a finite four-dimensional lattice of spatial volume $V = L^3$, compact extension L_0 , and spacing a . The fields satisfy periodic boundary conditions in the spatial directions and shifted

boundary conditions in the compact one

$$\begin{aligned} U_\mu(x_0 + L_0, \mathbf{x}) &= U_\mu(x_0, \mathbf{x} - L_0 \boldsymbol{\xi}), \\ \psi(x_0 + L_0, \mathbf{x}) &= -\psi(x_0, \mathbf{x} - L_0 \boldsymbol{\xi}), \\ \bar{\psi}(x_0 + L_0, \mathbf{x}) &= -\bar{\psi}(x_0, \mathbf{x} - L_0 \boldsymbol{\xi}), \end{aligned} \quad (1)$$

where $U_\mu \in \text{SU}(3)$ are the link variables, ψ and $\bar{\psi}$ are triplets in flavour space of degenerate quark fields, and the spatial vector $\boldsymbol{\xi}$ characterizes the moving frame in the Euclidean space-time [22–24].

The QCD lattice action is $S = S_G + S_F$, where S_G and S_F are the gluonic and the fermionic parts, respectively. The pure gauge action is discretized through the standard Wilson plaquette definition

$$S_G = \frac{6}{g_0^2} \sum_x \sum_{\mu < \nu} \left[1 - \frac{1}{3} \text{Re Tr} \{ U_{\mu\nu}(x) \} \right], \quad (2)$$

where the trace is over the color index, g_0 is the bare coupling constant, $U_{\mu\nu}(x)$ is the plaquette as defined in Ref. [16], $\mu, \nu = 0, \dots, 3$, and x is the space-time coordinate. The fermionic part of the action is

$$S_F = a^4 \sum_x \bar{\psi}(x) (D + m_0) \psi(x), \quad (3)$$

where m_0 is the bare quark mass and the $O(a)$ -improved lattice Dirac operator is $D = D_w + aD_{\text{sw}}$ [26, 27]. The massless Wilson-Dirac operator D_w and the Sheikholeslami-Wohlert operator D_{sw} are given in Ref. [16] where all unexplained notation adopted in this letter can be found. Finally, the partition function Z and the free energy density f are readily defined as

$$f = -\frac{1}{L_0 V} \ln Z, \quad Z = \int DUD\psi D\bar{\psi} e^{-S}, \quad (4)$$

where the integration measures on the various fields are defined as usual.

The key idea for reaching very high temperatures with a moderate computational effort is to renormalize the theory by fixing the value of a non-perturbatively defined coupling [15, 16]. The coupling can be defined in a finite volume and computed precisely and efficiently on the lattice for values of the renormalization scale μ which span several orders of magnitude by using step-scaling techniques [20, 28, 29]. To make a definite choice, we adopt the definition based on the Schrödinger functional (SF) $\bar{g}_{\text{SF}}^2(\mu)$ [30–32]. Once the renormalized coupling has been determined in the continuum limit for $\mu \sim T$ [28, 29], the theory at temperature T is renormalized by fixing the coupling at finite lattice spacing to be

$$\bar{g}_{\text{SF}}^2(g_0^2, a\mu) = \bar{g}_{\text{SF}}^2(\mu), \quad a\mu \ll 1. \quad (5)$$

This condition fixes the so-called lines of constant physics, i.e. the dependence of the bare coupling constant g_0^2 on the lattice spacing, for values of a at which

the scale μ and therefore T can be easily accommodated. As we change the physical temperature, we impose different renormalization conditions which, however, define the very same renormalized theory at all temperatures. Once the lines of constant physics have been fixed, we determine the values of the critical mass m_{cr} by requiring that the PCAC mass, computed in a finite volume with SF boundary conditions, vanishes [29]. As a consequence, at each T the theory can be simulated efficiently at various lattice spacings without suffering from large discretization errors, and the continuum limit of the observables can be taken with confidence. All technical details on how the renormalization procedure is implemented in practice and the values of the bare parameters of the lattices simulated are given in Appendices A and B of Ref. [16].

Entropy density in a moving frame — In the presence of shifted boundary conditions, the entropy density at finite lattice spacing can be defined as [22–24]

$$\frac{s}{T^3} = \frac{1 + \boldsymbol{\xi}^2}{\xi_k} \frac{1}{T^4} \frac{\Delta f_\xi}{\Delta \xi_k} \quad (6)$$

where $T = 1/(L_0 \sqrt{1 + \boldsymbol{\xi}^2})$, and the last term on the r.h.s. is a discrete derivative of the free-energy density with respect to the shift component in direction k . For computational efficiency, it is convenient to introduce the following decomposition at fixed g_0 and L_0/a

$$\frac{\Delta f_\xi}{\Delta \xi_k} = \frac{\Delta(f_\xi - f_\xi^\infty)}{\Delta \xi_k} + \frac{\Delta f_\xi^\infty}{\Delta \xi_k}, \quad (7)$$

where f_ξ^∞ is the free-energy density in the limit $m_q \rightarrow \infty$, and $m_q = m_0 - m_{\text{cr}}$ is the subtracted quark mass. By re-writing the first term on the r.h.s. of Eq. (7) as the integral of the derivative w.r.t. m_q , we have

$$\frac{\Delta(f_\xi - f_\xi^\infty)}{\Delta \xi_k} = -\frac{\Delta}{\Delta \xi_k} \int_{m_q}^{\infty} \frac{\partial f_\xi^{m_q}}{\partial m_q} = -\int_{m_q}^{\infty} \frac{\Delta(\bar{\psi}\psi)_\xi^{m_q}}{\Delta \xi_k}, \quad (8)$$

where $\int_{m_q}^{\infty} = \int_0^{\infty} dm_q$, and the last integral can be computed by performing numerical simulations of QCD at various quark masses, as we discuss below. The second term on the r.h.s. of Eq. (7) corresponds to the contribution in the static quark limit of QCD, i.e. in the SU(3) Yang–Mills theory, and it can be written as [33]

$$\frac{\Delta f_\xi^\infty}{\Delta \xi_k} = \frac{\Delta f_\xi^\infty}{\Delta \xi_k} \Big|_{g_0^2=0} - \int_0^{g_0^2} du \frac{1}{u} \frac{\Delta \langle S_G \rangle_\xi^\infty}{\Delta \xi_k} \Big|_{g_0^2=u}. \quad (9)$$

Although this contribution has the largest variance, it can be computed by pure gauge simulations which are orders of magnitude cheaper than those of QCD.

Numerical computation of s — We compute the entropy density in QCD with $N_f = 3$ massless quarks at

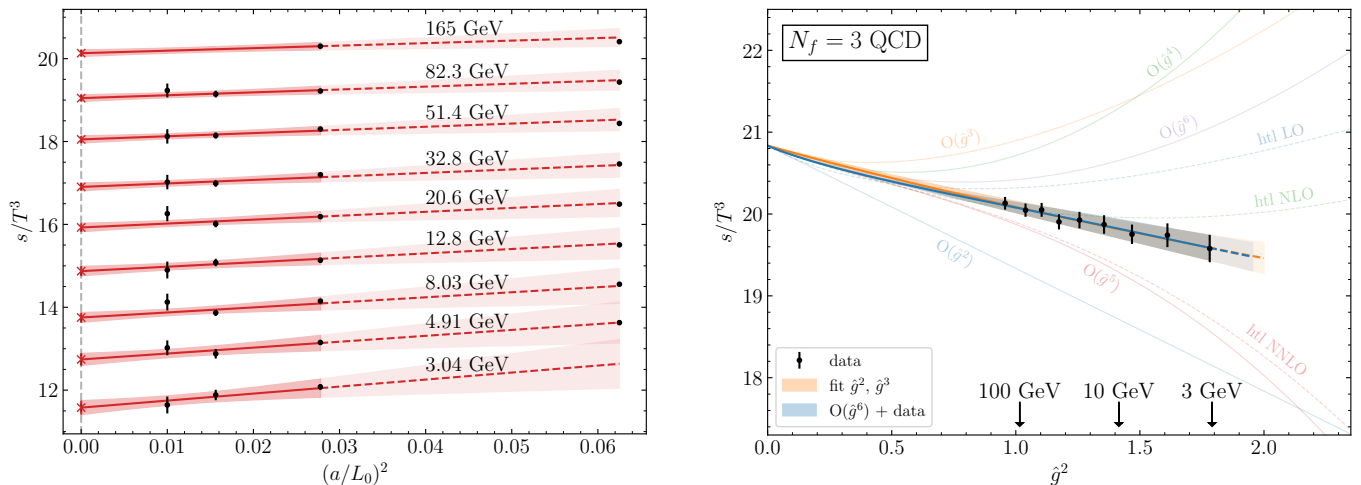


FIG. 1. Left: values of s/T^3 as a function of $(a/L_0)^2$ corresponding to T_n ($n = 0, \dots, 8$) shifted downward by n for better readability. Right: continuum values of s/T^3 versus $\hat{g}^2(T)$. The various continuous curves show the central values of the perturbative expressions in Ref. [12], each one including up to the order indicated on the curve. The analogous curves for hard-thermal-loop (htl) perturbation theory [34] are represented by dashed lines. The orange and the blue bands (grey when the two overlap) represent the results of the fits to Eqs. (11) and (12), respectively, as explained in the main text.

the 9 temperatures T_0, \dots, T_8 given in Table I which span the range from about 3 GeV up to 165 GeV. We adopt shifted boundary conditions in the compact direction with $\xi = (1, 0, 0)$ and, in order to extrapolate the results to the continuum limit with confidence, several lattice spacings are simulated at each temperature with the extension of the compact direction being $L_0/a = 4, 6, 8, 10$.

The inverse bare coupling constant $6/g_0^2$ and the critical quark mass are fixed at each lattice spacing by applying the renormalization strategy outlined above. The values of $6/g_0^2$ simulated are reported in Table II of Appendix C. The lattice size in the spatial directions has been set to $L/a = 144$ so that LT ranges from 10 to 25. We have explicitly checked that finite size effects in the entropy density are negligible within our statistical errors, see Appendix D for details.

The discrete derivatives in the shift are estimated by computing the chiral condensate and the expectation values of the gluon action at $\xi = (1 \pm 2a/L_0, 0, 0)$, so that each evaluation requires 2 different simulations. For each value of L_0/a and $6/g_0^2$,

T	$T(\text{GeV})$	s/T^3
T_0	165(6)	20.13(8)
T_1	82.3(2.8)	20.05(8)
T_2	51.4(1.7)	20.05(9)
T_3	32.8(1.0)	19.90(9)
T_4	20.6(6)	19.93(10)
T_5	12.8(4)	19.87(11)
T_6	8.03(22)	19.75(12)
T_7	4.91(13)	19.74(15)
T_8	3.04(8)	19.58(17)

TABLE I. Temperatures considered together with the results for s/T^3 in the continuum limit.

the integral in Eq. (8) is carried out by combining Gaussian quadratures as described in Appendix A which, altogether, require the computation of the derivative of the chiral condensate at 20 quark masses. The integral on the r.h.s. of Eq. (9) is computed from the the discrete derivative of the numerical estimate of $\langle S_G \rangle_{\xi}^{\infty}$ in the SU(3) Yang–Mills theory as discussed in Appendix B.

In the left panel of Figure 1 we show the one-loop perturbatively improved values, as defined in Appendix E, of s/T^3 . To extrapolate these results to the continuum limit, we have considered several fitting strategies which are discussed in detail in Appendix F. The best fit is the one where points at all temperatures and $L_0/a > 4$ are fitted together linearly in $(a/L_0)^2$ with a coefficient whose temperature dependence is proportional to $\bar{g}_{\text{SF}}^3(\sqrt{2}T)$ and with weights in the definition of χ^2 which take into account statistical and systematic errors. The resulting value of $\chi^2/\chi_{\text{exp}}^2$ is 0.82, where χ_{exp}^2 is defined as in Ref. [35]. Lattice artifacts turn out to be rather mild.

Our best values of s/T^3 in the continuum limit are reported in Table I and shown in the right panel of Figure 1 as a function of $\hat{g}^2(T)$. The latter is defined as the 5-loop strong coupling constant squared in the $\overline{\text{MS}}$ scheme at the renormalization scale $\mu = 2\pi T$. At the leading order, its well known expression reads

$$\frac{1}{\hat{g}^2(T)} \equiv \frac{9}{8\pi^2} \ln \frac{2\pi T}{\Lambda_{\overline{\text{MS}}}} + \dots, \quad (10)$$

where $\Lambda_{\overline{\text{MS}}} = 341$ MeV is taken from Ref. [36], while for the complete formula see Ref. [37, 38]. It is important

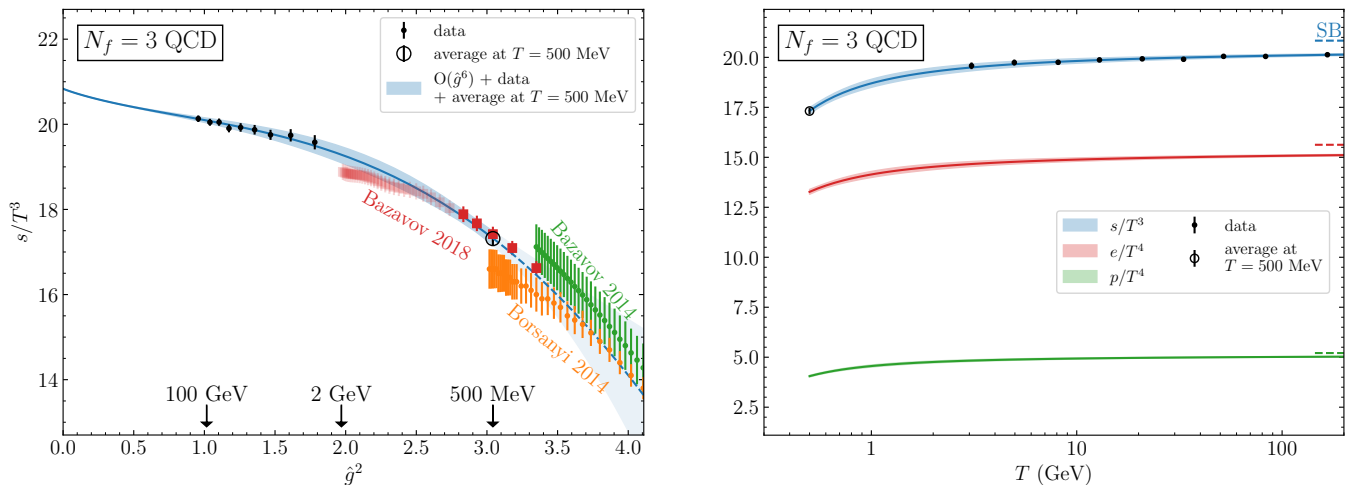


FIG. 2. Left: normalized entropy density, s/T^3 , versus $\hat{g}^2(T)$. The blue curve is our best parameterization of s/T^3 for $T \geq 500$ MeV. Data from Refs. [8–10] are also shown. Right: normalized pressure, entropy and energy densities as a function of temperature for $T \geq 500$ MeV.

to stress that for our purposes $\hat{g}^2(T)$ is just a function of the temperature T that we use to scrutinize in detail the temperature dependence of our results. Taken at face value, data point straight to the Stefan-Boltzmann (SB) value from which the point at the highest temperature differs by approximately 3%. The entropy density is indeed well represented by the phenomenological formula

$$\frac{s}{T^3} = \frac{32\pi^2}{45} \left[s_0 + s_2 \left(\frac{\hat{g}}{2\pi} \right)^2 + s_3 \left(\frac{\hat{g}}{2\pi} \right)^3 \right] \quad (11)$$

over the almost 2 orders of magnitude of the temperature range explored. If one opts for the simplest choice by forcing $s_3 = 0$, then the fit coefficients are $s_0 = 2.954(15)$ and $s_2 = -3.6(7)$ with the off diagonal elements of the covariant matrix being $\text{cov}(s_0, s_2)/[\sigma(s_0)\sigma(s_2)] = -0.84$. This result confirms that, when extrapolated to the $T \rightarrow \infty$ limit, the data point to the SB value, $s_0^{\text{SB}} = 2.969$, within errors. By enforcing $s_0 = s_0^{\text{SB}}$, the fit parameters are $s_2 = -5.1(9)$, $s_3 = 5(5)$ and the off diagonal element of the covariant matrix is $\text{cov}(s_2, s_3)/[\sigma(s_2)\sigma(s_3)] = -0.89$. The corresponding curve is shown in orange in the right panel of Figure 1. These analyses show that our data are compatible with a linear behaviour in $\hat{g}^2(T)$ but with a slope which tends to be different from the perturbative value -8.438 .

The Equation of State in the continuum — The known perturbative formulas suggest to parameterize the non-perturbative data with a polynomial interpolation of

the form

$$\frac{s}{T^3} = \frac{32\pi^2}{45} \sum_k s_k \left(\frac{\hat{g}}{2\pi} \right)^k. \quad (12)$$

By fixing the first coefficients to their perturbative values, $s_0 = 2.969$, $s_1 = 0$, $s_2 = -8.438$, $s_3 = 55.11$, $s_4 = -40.28 + 101.2 \ln(\hat{g}^2)$, $s_5 = -1174$, $s_6 = 4791 - 1629 \ln(\hat{g}^2) + q_c$ guarantees the expected behaviour of the normalized entropy density at asymptotically large temperatures [12]. As usual, we introduce the free coefficient q_c because there are unknown contributions at this order including those of non-perturbative origin in the three-dimensional effective theory. The last term that we include in the polynomial interpolation is of $O(\hat{g}^7)$. By fitting our data to the functional form in Eq. (12), we obtain $q_c = -5.1(1.7) \cdot 10^3$, $s_7 = 1.3(7) \cdot 10^4$ with $\text{cov}(q_c, s_7)/[\sigma(q_c)\sigma(s_7)] = -0.99$ and an excellent $\chi^2/\chi_{\text{exp}}^2 = 0.58$. The corresponding curve is shown in blue in the right panel of Figure 1 (grey when this curve overlaps with the orange one). If we force $s_7 = 0$, we obtain $q_c = -2.5(3) \cdot 10^3$ with $\chi^2/\chi_{\text{exp}}^2 = 1.52$. This analysis shows that contributions beyond the known perturbative ones are required to explain data even at these very large temperatures. For completeness it must be said that data are compatible with the results of hard-thermal-loop perturbation theory, albeit within the large systematic uncertainties quoted in Ref. [34]. A detailed discussion of this comparison will be reported in Ref. [38].

Discussion and conclusions — At much lower temperatures, up to 500 MeV or so, the entropy density with

$N_f = 2 + 1$ flavours has been determined in Refs. [8–10] with percent precision by extrapolating lattice data to the continuum limit. It is appropriate to compare their results with ours because the contribution due to the mass of the light quarks is at the permille level at 500 MeV [18], well below the errors quoted by the two collaborations. Albeit with very large errors, the best fit of our data in the previous section is compatible with the value of the normalized entropy density at 500 MeV, $s/T^3 = 17.31(16)$, obtained by averaging the two results from Refs. [8, 10]. We therefore combine the latter value with our data, and interpolate this enlarged data set with the polynomial given in Eq. (12). Again the first coefficients are fixed to their perturbative values, while a fit to the data gives $q_c = -4.0(1.1) \cdot 10^3$, $s_7 = 7(4) \cdot 10^3$ with the off diagonal element of the covariant matrix being $\text{cov}(q_c, s_7)/[\sigma(q_c)\sigma(s_7)] = -1.00$ and $\chi^2/\chi_{\text{exp}}^2 = 0.79$. This is our best parameterization of s/T^3 for QCD with $N_f = 3$ flavours for $T \geq 500$ MeV which has an error of at most 1% within that range. It is shown in blue in the left panel of Figure 2. Since s_7 turns out to be close to zero, for completeness we also provide the result $q_c = -2.02(6) \cdot 10^3$ of the fit obtained by fixing $s_7 = 0$ which has a $\chi^2/\chi_{\text{exp}}^2 = 2.64$. We notice that, when extended below 500 MeV, our best interpolation curve is compatible with the continuum extrapolated data in Refs. [8–10] given the large errors of the data, see left panel of Figure 2.

Once the entropy density is known, the pressure and the energy density can be computed by using the thermodynamic relations $s = \partial p/\partial T$ and $e = Ts - p$, respectively. Following Ref. [12], the results for the pressure and the energy density can be parameterized analogously to Eq. (12) with $p_7 = s_7 + (5b_0p_5 + 3b_1p_3)/4$, where $b_0 = 9/4$, $b_1 = 4$, and p_3 and p_5 can be found in Ref. [12]. The corresponding curves are shown in the right panel of Figure 2 for $T \geq 500$ MeV.

The strategy introduced here has paved the way to determine the EoS of QCD up to temperatures of the order of the electro-weak scale. The numerical results presented here can indeed be systematically improved in the future by investing more computational resources. As a final remark, we notice that the strategy can be straightforwardly extended to QCD with 4 and 5 (massive) quarks.

Acknowledgments — We acknowledge Leonardo Cosmai for useful discussions. We acknowledge PRACE for awarding us access to the HPC system MareNostrum4 at the Barcelona Supercomputing Center (Proposals n. 2018194651 and 2021240051) where some of the numerical results presented in this letter have been obtained. We also thank CINECA for providing us with a very generous access to Leonardo during the early phases of operations of the machine and for the computer time allocated via the CINECA-INFN, CINECA-Bicocca agreements. The R&D has been carried out on the PC clusters

Wilson and Knuth at Milano-Bicocca. We thank all these institutions for the technical support. This work is (partially) supported by ICSC – Centro Nazionale di Ricerca in High Performance Computing, Big Data and Quantum Computing, funded by European Union – NextGenerationEU.

-
- [1] S. Navas *et al.* (Particle Data Group), Review of particle physics, *Phys. Rev. D* **110**, 030001 (2024).
 - [2] K. Saikawa and S. Shirai, Primordial gravitational waves, precisely: The role of thermodynamics in the Standard Model, *JCAP* **05**, 035, arXiv:1803.01038 [hep-ph].
 - [3] M. Hindmarsh and O. Philipsen, WIMP dark matter and the QCD equation of state, *Phys. Rev. D* **71**, 087302 (2005), arXiv:hep-ph/0501232.
 - [4] M. Drees, F. Hajkarim, and E. R. Schmitz, The Effects of QCD Equation of State on the Relic Density of WIMP Dark Matter, *JCAP* **06**, 025, arXiv:1503.03513 [hep-ph].
 - [5] K. Saikawa and S. Shirai, Precise WIMP Dark Matter Abundance and Standard Model Thermodynamics, *JCAP* **08**, 011, arXiv:2005.03544 [hep-ph].
 - [6] S. Borsanyi *et al.*, Calculation of the axion mass based on high-temperature lattice quantum chromodynamics, *Nature* **539**, 69 (2016), arXiv:1606.07494 [hep-lat].
 - [7] G. Grilli di Cortona, E. Hardy, J. Pardo Vega, and G. Villadoro, The QCD axion, precisely, *JHEP* **01**, 034, arXiv:1511.02867 [hep-ph].
 - [8] S. Borsanyi, Z. Fodor, C. Hoelbling, S. D. Katz, S. Krieg, and K. K. Szabo, Full result for the QCD equation of state with 2+1 flavors, *Phys. Lett. B* **730**, 99 (2014), arXiv:1309.5258 [hep-lat].
 - [9] A. Bazavov *et al.* (HotQCD), Equation of state in (2+1)-flavor QCD, *Phys. Rev. D* **90**, 094503 (2014), arXiv:1407.6387 [hep-lat].
 - [10] A. Bazavov, P. Petreczky, and J. H. Weber, Equation of State in 2+1 Flavor QCD at High Temperatures, *Phys. Rev. D* **97**, 014510 (2018), arXiv:1710.05024 [hep-lat].
 - [11] A. D. Linde, Infrared Problem in Thermodynamics of the Yang-Mills Gas, *Phys. Lett. B* **96**, 289 (1980).
 - [12] K. Kajantie, M. Laine, K. Rummukainen, and Y. Schroder, The Pressure of hot QCD up to $g^6 \ln(1/g)$, *Phys. Rev. D* **67**, 105008 (2003), arXiv:hep-ph/0211321.
 - [13] P. Navarrete and Y. Schröder, The g^6 pressure of hot Yang-Mills theory: Canonical form of the integrand, (2024), arXiv:2408.15830 [hep-ph].
 - [14] S. Borsanyi, G. Endrodi, Z. Fodor, S. D. Katz, and K. K. Szabo, Precision SU(3) lattice thermodynamics for a large temperature range, *JHEP* **07**, 056, arXiv:1204.6184 [hep-lat].
 - [15] L. Giusti and M. Pepe, Equation of state of the SU(3) Yang–Mills theory: A precise determination from a moving frame, *Phys. Lett.* **B769**, 385 (2017), arXiv:1612.00265 [hep-lat].
 - [16] M. Dalla Brida, L. Giusti, T. Harris, D. Laudicina, and M. Pepe, Non-perturbative thermal QCD at all temperatures: the case of mesonic screening masses, *JHEP* **04**, 034, arXiv:2112.05427 [hep-lat].
 - [17] L. Giusti, T. Harris, D. Laudicina, M. Pepe, and P. Rescigno, Baryonic screening masses in QCD at high temperature, *Phys. Lett. B* **855**, 138799 (2024),

- arXiv:2405.04182 [hep-lat].
- [18] M. Laine and Y. Schroder, Quark mass thresholds in QCD thermodynamics, *Phys. Rev. D* **73**, 085009 (2006), arXiv:hep-ph/0603048.
- [19] M. Lüscher, P. Weisz, and U. Wolff, A Numerical method to compute the running coupling in asymptotically free theories, *Nucl. Phys. B* **359**, 221 (1991).
- [20] M. Lüscher, R. Sommer, P. Weisz, and U. Wolff, A Precise determination of the running coupling in the SU(3) Yang-Mills theory, *Nucl. Phys. B* **413**, 481 (1994), arXiv:hep-lat/9309005.
- [21] K. Jansen, C. Liu, M. Lüscher, H. Simma, S. Sint, R. Sommer, P. Weisz, and U. Wolff, Nonperturbative renormalization of lattice QCD at all scales, *Phys. Lett. B* **372**, 275 (1996), arXiv:hep-lat/9512009.
- [22] L. Giusti and H. B. Meyer, Thermal momentum distribution from path integrals with shifted boundary conditions, *Phys. Rev. Lett.* **106**, 131601 (2011), arXiv:1011.2727 [hep-lat].
- [23] L. Giusti and H. B. Meyer, Thermodynamic potentials from shifted boundary conditions: the scalar-field theory case, *JHEP* **11**, 087, arXiv:1110.3136 [hep-lat].
- [24] L. Giusti and H. B. Meyer, Implications of Poincare symmetry for thermal field theories in finite-volume, *JHEP* **01**, 140, arXiv:1211.6669 [hep-lat].
- [25] M. Dalla Brida, L. Giusti, and M. Pepe, Non-perturbative definition of the QCD energy-momentum tensor on the lattice, *JHEP* **04**, 043, arXiv:2002.06897 [hep-lat].
- [26] K. G. Wilson, Confinement of Quarks, *Phys. Rev. D* **10**, 2445 (1974).
- [27] B. Sheikholeslami and R. Wohlert, Improved Continuum Limit Lattice Action for QCD with Wilson Fermions, *Nucl. Phys.* **B259**, 572 (1985).
- [28] M. Dalla Brida, P. Fritzsche, T. Korzec, A. Ramos, S. Sint, and R. Sommer (ALPHA), Determination of the QCD Λ -parameter and the accuracy of perturbation theory at high energies, *Phys. Rev. Lett.* **117**, 182001 (2016), arXiv:1604.06193 [hep-ph].
- [29] M. Dalla Brida, P. Fritzsche, T. Korzec, A. Ramos, S. Sint, and R. Sommer (ALPHA), A non-perturbative exploration of the high energy regime in $N_f = 3$ QCD, *Eur. Phys. J. C* **78**, 372 (2018), arXiv:1803.10230 [hep-lat].
- [30] M. Lüscher, R. Narayanan, P. Weisz, and U. Wolff, The Schrödinger functional: A Renormalizable probe for non-Abelian gauge theories, *Nucl. Phys. B* **384**, 168 (1992), arXiv:hep-lat/9207009.
- [31] S. Sint, On the Schrodinger functional in QCD, *Nucl. Phys. B* **421**, 135 (1994), arXiv:hep-lat/9312079.
- [32] S. Sint and R. Sommer, The Running coupling from the QCD Schrodinger functional: A One loop analysis, *Nucl. Phys. B* **465**, 71 (1996), arXiv:hep-lat/9508012.
- [33] L. Giusti and M. Pepe, Energy-momentum tensor on the lattice: Nonperturbative renormalization in Yang-Mills theory, *Phys. Rev. D* **91**, 114504 (2015), arXiv:1503.07042 [hep-lat].
- [34] J. O. Andersen, L. E. Leganger, M. Strickland, and N. Su, Three-loop HTL QCD thermodynamics, *JHEP* **08**, 053, arXiv:1103.2528 [hep-ph].
- [35] M. Bruno and R. Sommer, On fits to correlated and auto-correlated data, *Comput. Phys. Commun.* **285**, 108643 (2023), arXiv:2209.14188 [hep-lat].
- [36] M. Bruno, M. Dalla Brida, P. Fritzsche, T. Korzec, A. Ramos, S. Schaefer, H. Simma, S. Sint, and R. Sommer (ALPHA), QCD Coupling from a Nonperturbative Determination of the Three-Flavor Λ Parameter, *Phys. Rev. Lett.* **119**, 102001 (2017), arXiv:1706.03821 [hep-lat].
- [37] P. A. Baikov, K. G. Chetyrkin, and J. H. Kühn, Five-Loop Running of the QCD coupling constant, *Phys. Rev. Lett.* **118**, 082002 (2017), arXiv:1606.08659 [hep-ph].
- [38] M. Bresciani, M. Dalla Brida, L. Giusti, and M. Pepe, in preparation.
- [39] N. Husung, P. Marquard, and R. Sommer, Asymptotic behavior of cutoff effects in Yang-Mills theory and in Wilson's lattice QCD, *Eur. Phys. J. C* **80**, 200 (2020), arXiv:1912.08498 [hep-lat].
- [40] N. Husung, P. Marquard, and R. Sommer, The asymptotic approach to the continuum of lattice QCD spectral observables, *Phys. Lett. B* **829**, 137069 (2022), arXiv:2111.02347 [hep-lat].
- [41] N. Husung, Logarithmic corrections to $O(a)$ and $O(a^2)$ effects in lattice QCD with Wilson or Ginsparg-Wilson quarks, *Eur. Phys. J. C* **83**, 142 (2023), [Erratum: *Eur.Phys.J.C* 83, 144 (2023)], arXiv:2206.03536 [hep-lat].
- [42] F. Joswig, S. Kuberski, J. T. Kuhlmann, and J. Neuenendorf, pyerrors: A python framework for error analysis of Monte Carlo data, *Comput. Phys. Commun.* **288**, 108750 (2023), arXiv:2209.14371 [hep-lat].
- [43] A. Ramos, Automatic differentiation for error analysis of Monte Carlo data, *Comput. Phys. Commun.* **238**, 19 (2019), arXiv:1809.01289 [hep-lat].

Appendices

Appendix A: Integration in the bare mass —

The numerical computation of the integral in the bare subtracted quark mass of Eq. (8) is carried out as follows. At fixed values of L_0/a and g_0^2 we split the integration in three intervals of bare mass $\{0 \leq m_q/T < 5\}$, $\{5 \leq m_q/T < \tilde{m}\}$ and $\{\tilde{m} \leq m_q/T < \infty\}$, where $\tilde{m} = 35$ for $L_0/a = 4$ and $\tilde{m} = 20$ for $L_0/a = 6, 8, 10$. The integrals in the first two domains are computed with 10-point and 7-point Gaussian quadratures, respectively. After a change of variable to the hopping parameter $\kappa = 1/(2am_0 + 8)$, which makes the third domain compact, the integral is computed with a 3-point Gaussian quadrature. This optimized integration scheme has been chosen using tree-level perturbation theory as guidance so that systematic effects from the numerical quadratures are negligible with respect to the target statistical accuracy. We then checked explicitly on the non-perturbative data that the systematic effects from the numerical quadratures are negligible by using the Gauss-Kronrod quadrature on a selected set of lattices, i.e. that the addition of points does not affect the result of the integral within errors.

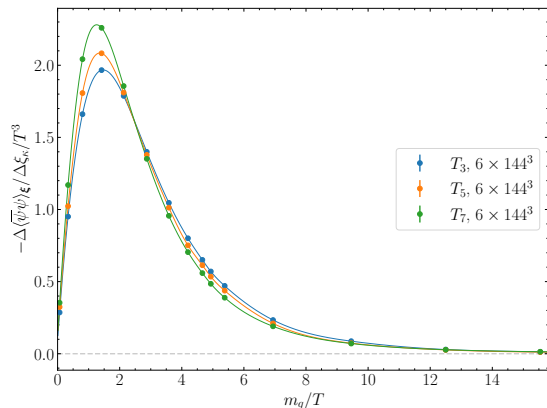


FIG. 3. Derivative in the shift of the chiral condensate as a function of m_q/T at some selected bare parameters. Points have been interpolated with a cubic spline to guide the eye. Error bars are smaller than the markers.

Figure 3 shows the integrand function as obtained from lattice simulations. Each point in the plot comes from two independent ensembles with shifts $\xi = (1 \pm 2a/L_0, 0, 0)$ at the same bare parameters (see main text).

Appendix B: Integration in the bare coupling —

At fixed L_0/a , the integration in the bare coupling appearing in the right side of Eq. (9) has to be performed in the intervals $g_0^2 \in [0, g_0^2|_{T_i}]$, $i = 0, \dots, 8$, where $g_0^2|_{T_i}$ are the bare couplings at given temperature T_i whose corresponding inverse values $6/g_0^2$ are reported in Table II. The integrals have been split into several parts. For the first segment, $[0, 6/15]$, we applied the 2-point trapezoidal rule (3-point Simpson rule for $L_0/a = 4$) and

a 3-point Gaussian quadrature has been employed in the range $[6/15, 6/9]$. In the domain $[6/9, g_0^2|_{T_0}]$ we adopted a 3-point Gaussian quadrature for $L_0/a = 4$, and the midpoint rule for $L_0/a = 6$. The interval $[6/9, g_0^2|_{T_1}]$ has been integrated with a 3-point Gaussian quadrature, as well as the domains $[g_0^2|_{T_{i-1}}, g_0^2|_{T_i}]$ with $i = 2, \dots, 6$. Finally, for the last two intervals $i = 7, 8$ a 5-point Gaussian integration has been chosen. These evaluations require the sampling of the integrand function, $\Delta \langle S_G \rangle_\xi^\infty / \Delta \xi_k$, at several values of bare coupling, prescribed by the quadrature rules. At each value of g_0^2 the integrand function is estimated with two independent numerical simulations of the pure SU(3) Yang-Mills theory at the same bare parameters and shifts $\xi = (1 \pm 2a/L_0, 0, 0)$.

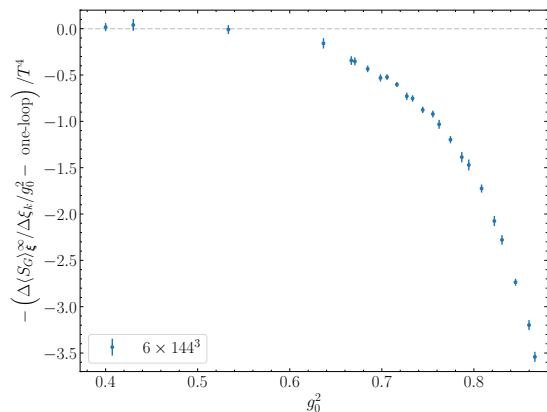


FIG. 4. Derivative in the shift of the pure gauge action as a function of g_0^2 for $L_0/a = 6$. For convenience we subtracted from the data the result at one-loop order in lattice perturbation theory.

Figure 4 shows the resulting integrand for the $L_0/a = 6$ case, where its one-loop value has been subtracted. Notice that at values of the squared coupling below $g_0^2 = 0.5$ the integrand is well compatible with the perturbative prediction to which it can be safely connected.

Appendix C: Monte Carlo results — In Table II we give the values of $\frac{\Delta f_\xi^\infty}{\Delta \xi_k}$ and $\frac{\Delta(f_\xi - f_\xi^\infty)}{\Delta \xi_k}$ for each lattice simulated together with the extension of the compact direction, L_0/a , and the inverse bare gauge coupling, $6/g_0^2$.

Appendix D: Finite volume effects — At high temperature finite volume effects in the entropy are exponentially suppressed for $L \rightarrow \infty$ with an exponent $\propto LT$ [16, 24]. Since in our simulations $10 \lesssim LT \lesssim 25$, we expect these effects to be very small, well below the statistical uncertainties. We have explicitly checked this at the temperatures T_1 and T_8 for $L_0/a = 6$.

The determination of the entropy density using Eq. (6) on volumes much larger than $L/a = 144$ would be computationally very demanding. For checking finite volume

L_0/a	$6/g_0^2$	$\frac{\Delta f_{\xi}^{\infty}}{\Delta \xi_k} \times 10^4$	$\frac{\Delta(f_{\xi} - f_{\xi}^{\infty})}{\Delta \xi_k} \times 10^4$	$6/g_0^2$	$\frac{\Delta f_{\xi}^{\infty}}{\Delta \xi_k} \times 10^4$	$\frac{\Delta(f_{\xi} - f_{\xi}^{\infty})}{\Delta \xi_k} \times 10^4$	$6/g_0^2$	$\frac{\Delta f_{\xi}^{\infty}}{\Delta \xi_k} \times 10^4$	$\frac{\Delta(f_{\xi} - f_{\xi}^{\infty})}{\Delta \xi_k} \times 10^4$
	T_0			T_1			T_2		
4	8.7325	37.861(24)	111.19(4)	8.3033	37.558(24)	110.73(4)	7.9794	37.260(24)	110.29(5)
6	8.9950	6.819(24)	15.25(5)	8.5403	6.768(24)	15.15(3)	8.2170	6.720(24)	15.24(4)
8	-	-	-	8.7325	2.078(9)	4.370(24)	8.4044	2.062(9)	4.381(22)
10	-	-	-	8.8727	0.856(11)	1.740(19)	8.5534	0.850(11)	1.731(19)
	T_3			T_4			T_5		
4	7.6713	36.890(24)	109.98(6)	7.3534	36.381(24)	109.69(5)	7.0250	35.625(25)	109.31(6)
6	7.9091	6.656(24)	15.14(4)	7.5909	6.564(24)	15.15(4)	7.2618	6.423(24)	15.16(4)
8	8.0929	2.041(9)	4.347(24)	7.7723	2.010(9)	4.379(24)	7.4424	1.964(9)	4.439(27)
10	8.2485	0.843(11)	1.725(20)	7.9322	0.830(11)	1.766(21)	7.6042	0.813(11)	1.737(24)
	T_6			T_7			T_8		
4	6.7079	34.499(25)	109.30(6)	6.3719	32.397(25)	109.92(9)	-	-	-
6	6.9433	6.201(24)	15.30(5)	6.6050	5.767(24)	15.61(5)	6.2735	4.711(26)	16.43(7)
8	7.1254	1.890(9)	4.436(22)	6.7915	1.748(9)	4.57(4)	6.4680	1.416(9)	4.89(4)
10	7.2855	0.784(11)	1.793(24)	6.9453	0.722(11)	1.839(20)	6.6096	0.571(11)	1.939(23)

TABLE II. Results for $\frac{\Delta f_{\xi}^{\infty}}{\Delta \xi_k}$ and $\frac{\Delta(f_{\xi} - f_{\xi}^{\infty})}{\Delta \xi_k}$ obtained from Monte Carlo simulations. For each lattice we also report the size of the compact direction, L_0/a , and the value of the inverse bare gauge coupling, $6/g_0^2$.

T	L/a	$\langle T_{01}^{G,\{6\}} \rangle_{\xi} \times 10^3$	$\langle T_{01}^{F,\{6\}} \rangle_{\xi} \times 10^3$
T_1	144	-0.541(3)	-1.2164(11)
	288	-0.539(3)	-1.2183(11)
T_8	144	-0.458(4)	-1.1280(19)
	288	-0.455(4)	-1.1317(20)

TABLE III. Expectation values of the bare EMT matrix elements. We consider two values of the spatial volume for $L_0/a = 6$ at T_1 and T_8 .

effects we employ the relation [24, 25]

$$\frac{s}{T^3} = -\frac{1 + \xi^2}{\xi_k} \frac{1}{T^4} \langle T_{0k}^{R,\{6\}} \rangle_{\xi}, \quad (13)$$

where we define the sextet component of the renormalized energy-momentum tensor as [25]

$$T_{\mu\nu}^{R,\{6\}} = Z_G^{\{6\}}(g_0^2) T_{\mu\nu}^{G,\{6\}} + Z_F^{\{6\}}(g_0^2) T_{\mu\nu}^{F,\{6\}}. \quad (14)$$

We computed the bare matrix elements of the energy-momentum tensor at two values of the spatial size $L/a = 144$ and $L/a = 288$, on $L_0/a = 6$ lattices at the bare parameters of T_1 , T_8 and shift $\xi = (1, 0, 0)$. The results are reported in Table III. No finite size effects are observed in the bare matrix elements. The statistical precision of the bare matrix elements has been tuned so that the relative error on the entropy from Eq. (13), with the renormalization constants estimated in perturbation theory, is comparable with the one obtained from the results in Table II.

Appendix E: Perturbative improvement — At fixed parameters L_0/a and g_0 we remove the lattice artifacts at one-loop order in lattice perturbation theory through

the replacement,

$$s(L_0/a, g_0^2) \rightarrow s(L_0/a, g_0^2) \cdot \frac{s_0 + s_2 \left(\frac{g}{2\pi}\right)^2}{s_0(L_0/a) + s_2(L_0/a) \left(\frac{g}{2\pi}\right)^2}, \quad (15)$$

where $g^2 = \bar{g}_{\text{SF}}^2(1/L_0)$ and in the denominator we have the one-loop coefficients in lattice perturbation theory in the thermodynamic limit. Their values for the relevant

L_0/a	4	6	8	10	∞
s_0	4.719	3.438	3.145	3.059	2.969
s_2	-23.465	-13.085	-9.955	-9.089	-8.438

TABLE IV. Coefficients for the one-loop improvement of the lattice entropy density.

L_0/a are listed in Table IV, together with the results in the continuum limit. After improving at one-loop order, the leading discretization effects are expected to be parametrically of $O(g^3 a^2)$, since all $O(g^0 a^n)$ and $O(g^2 a^n)$ effects have been subtracted. On general grounds, at finite temperature we expect odd powers in the coupling to be present.

Appendix F: Continuum limit extrapolations

We estimated the entropy density in the continuum limit by performing a combined fit of the data at the various temperatures at finite lattice spacing. We have considered the following fit function

$$s(T_i)/T_i^3 = c_i + d_2 g_i^3 (a/L_0)^2 + d_3 g_i^3 (a/L_0)^3, \quad (16)$$

where $i = 0, \dots, 8$, $g_i \equiv \bar{g}_{\text{SF}}(\sqrt{2}T_i)$, c_i are the continuum values, and d_2, d_3 parameterize the discretization effects. We first considered fits to the data with $L_0/a = 4, 6, 8, 10$, where either $d_3 = 0$ or $d_3 \neq 0$. Both fits have $\chi^2/\chi_{\text{exp}}^2 \approx$

1, with the former giving values for c_i which are statistically 3-4 times more precise. Although compatible within the larger errors of the second fit, the extrapolated central values of the first fit are systematically higher. We then compared the fit with $L_0/a \geq 4$ and $d_3 \neq 0$ to the one with $L_0/a > 4$ and $d_3 = 0$. For the latter we get $\chi^2/\chi_{\text{exp}}^2 \approx 0.7$ and comparable errors for the c_i . The two fits are in good agreement with no clear systematic difference. This hints to the fact that the data at $L_0/a = 4$ are likely affected by discretization effects of higher order than a^2 . To be conservative, we thus used the data with $L_0/a = 4$ only to estimate the size of the $O(a^3)$ contributions and included these as a systematic error to the points at finer lattice spacing. More precisely, we used the value of d_3 determined above, and modified the weights of the fits by adding in quadrature to the statistical errors of the points a systematic effect $d_3 g_i^3 (a/L_0)^3$. The final best fit is the one considering data with $L_0/a > 4$, $d_3 = 0$ in the fit ansatz Eq. (16), and the modified weights. The continuum re-

sults are stable against adding a term $\propto g_i^4 (a/L_0)^2$ to Eq. (16). To further corroborate the robustness of the fit we also checked the impact of logarithmic corrections to the $O(a^2)$ effects, modeled as $a^2 [\bar{g}_{\text{SF}}^2(\pi/a)]^\gamma$ [39–41]. By varying the effective anomalous dimension $\gamma \in [-1, 1]$ the results change by less than 1 standard deviation.

As an additional test for the soundness of the procedure, we repeated the whole analysis replacing $d_3 g_i^3 (a/L_0)^3$ with $d_4 g_i^3 (a/L_0)^4$ in Eq. (16). We obtain perfectly compatible results for the c_i with errors that are 10-20% smaller. Similar conclusions hold when replacing $g_i^3 \rightarrow g_i^4$ in both a^2 and a^3 terms.

All statistical correlations have been properly taken into account in the final results using the tools of Refs. [42, 43] for the error propagation. In particular, we propagated the statistical uncertainties deriving from the definition of the lines of constant physics [16, 29], and the correlations introduced by the integration in the bare coupling. While the former have a negligible effect on the errors of the final c_i values, neglecting the latter gives errors that would be about 10-20% smaller.